

A first step towards a direct inversion of the Lyman forest in QSO spectra

Adi Nusser¹ and Martin Haehnelt²

¹*Max-Planck-Institut für Astrophysik, Karl-Schwarzschild-Str. 1, D-85740 Garching b. München, Germany*

²*Institute of Astronomy, Madingley Rd, CB3-0HA, Cambridge, UK*

9 November 2021

ABSTRACT

A method for the recovery of the real space line-of-sight mass density field from Lyman absorption in QSO spectra is presented. The method makes use of a Lucy-type algorithm for the recovery of the H I density. The matter density is inferred from the H I density assuming that the absorption is due to a photoionized intergalactic medium which traces the mass distribution as suggested by recent numerical simulations. Redshift distortions are corrected iteratively from a simultaneous estimate of the peculiar velocity. The method is tested with mock spectra obtained from N-body simulations. The density field is recovered reasonably well up to densities where the absorption features become strongly saturated. The method is an excellent tool to study the density probability distribution and clustering properties of the mass density in the (mildly) non-linear regime. Combined with redshift surveys along QSO sightlines the method will make it possible to relate the clustering of high-redshift galaxies to the clustering of the underlying mass density. We further show that accurate estimates for $(\Omega_{\text{bar}} h^2)^2 J^{-1} H(z)^{-1}$ and higher order moments of the density probability function can be obtained despite the missing high density tail of the density distribution if a parametric form for the probability distribution of the mass density is assumed.

Key words: cosmology: theory, observation, dark matter, large-scale structure of the Universe — intergalactic medium — quasars: absorption lines

1 INTRODUCTION

The Lyman forest in QSO absorption spectra is now generally believed to be due to absorption by large-scale neutral hydrogen (H I) density fluctuations of moderate amplitude in a warm photoionized intergalactic medium (IGM). This relatively new paradigm for the Ly α forest differs considerably from the conventional “cloud” picture which had been advocated for two decades and in which the Lyman forest is due to a superposition from discrete absorbers with small cross sections (see Rauch 1998 for a review). The new picture had been investigated using analytical calculations (e.g. Bond, Szalay & Silk; Mc Gill 1990; Bi, Börner & Chu 1992) but was only generally accepted after the coherence length of the absorbing structure could be measured accurately and turned out to be of order several hundred kpc (Dinshaw et al. 1994, e.g. Bechtold et al. 1994). The picture was then further sustained by (hydrodynamical) cosmological simulations of gas in dark-matter dominated universes (Cen et al. 1994; Petitjean, Mückel & Kates 1995; Zhang, Anninos & Norman 1995; Hernquist et al. 1996; Miralda-Escudé et al. 1996). Important results of these simulations are a tight

correlation between the H I and the dark matter distribution (on scales larger than the Jeans length of the IGM) and a simple temperature-density relation for the IGM which depends only on the reionization history of the universe (e.g. Hui & Gnedin 1997, Haehnelt & Steinmetz 1998).

As a consequence of this new picture the Lyman forest can be used to probe the distribution and clustering of dark matter at high redshift. For example, Bi & Davidsen (1997) have developed a simple analytic model for the IGM to generate artificial QSO absorption spectra for a variant of the cold dark matter (CDM) cosmogony. They were able to reproduce the characteristic properties of observed absorption spectra. Croft et al. (1998) showed that absorption spectra provide important information on the shape and the amplitude of the power spectrum of mass fluctuations. Croft et al. used the following procedure. They first obtained a linearized flux distribution by applying the Gaussianization scheme proposed by Weinberg (1992). They then inferred the shape of the linear power spectrum of dark matter density fluctuation from the power spectrum of the linearized flux and used mock spectra from numerical simulations to determine the amplitude of the power spectrum. Gnedin &

Hui (1998) used mock spectra generated from simulations of collisionless particles run with a particle-Mesh code modified to mimic pressure effects of the gas to investigate the effect of amplitude and the power spectrum of dark-matter fluctuations on the column density distribution of Ly α absorption systems.

In this paper a complementary approach is taken. We propose to use an analytical model of the IGM for a direct inversion of the absorption features in QSO spectra. This approach has the advantage that no particular cosmological model has to be assumed. Furthermore, the actual real space density along the LOS and its probability distribution can be studied and a direct link to other observations is possible.

The paper is organized as follows. In Section 2 we describe the assumed model for the Lyman absorption. Section 3 presents the inversion algorithm for recovering the *real* space dark matter (DM) density along the l.o.s., concentrating on the Ly α forest. In section 4 we test the inversion procedure with mock spectra generated from numerical simulations of collisional dark matter and show how to estimate higher order moments of the density probability distribution and $(\Omega_{\text{bar}} h^2)^2 J^{-1} H(z)^{-1}$ (the parameter combination of baryonic density $\Omega_{\text{bar}} h^2$, ionizing flux J and Hubble constant $H(z)$ which determines the mean flux level in QSO absorption spectra). In section 5 we discuss possible applications and give our conclusions.

2 LYMAN ABSORPTION BY A PHOTOIONIZED INTERGALACTIC MEDIUM

Absorption spectra are normally presented in the form of a normalized flux which (neglecting noise and instrumental broadening) can be related to the optical depth as

$$F(w) = I_{\text{obs}}(w)/I_{\text{cont}}(w) = e^{-\tau(w)}, \quad (1)$$

where τ is the optical depth, w is the redshift space coordinate, $I_{\text{obs}}(w)$ is the observed flux and $I_{\text{cont}}(w)$ is the flux emitted from the quasar which would be observed without intervening absorption and has to be estimated from the data as well.

The optical depth in redshift space due to resonant Ly α scattering is related to the neutral hydrogen density, n_{HI} , along the line-of-sight (l.o.s) in real space as (Gunn & Peterson 1965, Bahcall & Salpeter 1965)

$$\tau(w) = \sigma_0 \frac{c}{H(z)} \int_{-\infty}^{\infty} n_{\text{HI}}(x) \mathcal{H}[w - x - v_{\text{p}}(x), b(x)] dx, \quad (2)$$

where σ_0 is the effective cross section for resonant line scattering, $H(z)$ is the Hubble constant at redshift z , x is the real space coordinate (in km s^{-1}), \mathcal{H} is the Voigt profile normalized such that $\int \mathcal{H} dx = 1$, $v_{\text{p}}(x)$ is the l.o.s. peculiar velocity, and $b(x)$ is the Doppler parameter due to thermal/turbulent broadening. For moderate optical depths the Voigt profile is well approximated by a Gaussian, $\mathcal{H} = \frac{1}{\sqrt{\pi} b} \exp[-(w - x - v_{\text{p}}(x))^2/b^2]$. Assuming that hydrogen is highly ionized and in photoionization equilibrium ($n_{\text{HI}} \propto n_{\text{H}}^2 J^{-1}$) we have

$$n_{\text{HI}} = \hat{n}_{\text{HI}} \left(\frac{n_{\text{H}}(\mathbf{x})}{\bar{n}_{\text{H}}} \right)^{\alpha} = \hat{n}_{\text{HI}} \left(\frac{\rho(\mathbf{x})}{\bar{\rho}} \right)^{\alpha}, \quad (3)$$

where \hat{n}_{HI} is the neutral hydrogen density at mean total gas density and $1.56 < \alpha < 2$ (Hui & Gnedin 1997). The second relation assumes that the gas density traces the dark matter density. At the low densities considered here shock heating is not important and the gas is at the photoionization equilibrium temperature. The Doppler parameter can then be related to the total gas density and temperature as

$$b(x) = 13 \left(\frac{\hat{T}}{10^4 \text{ K}} \right)^{0.5} \left(\frac{\rho_{\text{DM}}(\mathbf{x})}{\bar{\rho}_{\text{DM}}} \right)^{\beta} \text{ km s}^{-1}, \quad (4)$$

where \hat{T} is the temperature at the mean density and $0 < \beta < 0.31$ (Hui & Gnedin 1997).

Combining equation (2), (3) and (4) we get

$$\begin{aligned} \tau(w) &= \mathcal{A}(z) \int_{-\infty}^{\infty} \left(\frac{\rho_{\text{DM}}(\mathbf{x})}{\bar{\rho}_{\text{DM}}} \right)^{\alpha} \mathcal{H}[w - x - v_{\text{p}}(x), b(x)] dx \quad (5) \\ \mathcal{A}(z) &= \sigma_0 \frac{c}{H(z)} \hat{n}_{\text{HI}} \\ &\sim 0.12 h^{-1} \Omega_{\text{mat}}^{-0.5} \left(\frac{\Omega_{\text{bar}} h^2}{0.0125} \right)^2 \times \\ &\quad \left(\frac{\Gamma}{10^{-12} \text{ s}^{-1}} \right)^{-1} \left(\frac{\hat{T}}{10^4 \text{ K}} \right)^{-0.7} \left(\frac{1+z}{4} \right)^{4.5}. \end{aligned} \quad (6)$$

where Ω_{bar} and Ω_{mat} are the baryonic and total matter density in terms of the critical density and Γ is the photoionization rate per hydrogen atom (Γ is related to the flux of ionizing radiation J_{ν} as $\Gamma = 4\pi \int d\nu \sigma_{\nu} J_{\nu}/h\nu$, where σ_{ν} is the hydrogen absorption cross section). To obtain the second relation in equation (6) we have taken $\alpha_{\text{rec}} = 4.7 \times 10^{-13} (T/10^4 \text{ K})^{-0.7} \text{ cm}^{-3} \text{ s}^{-1}$ for the hydrogen recombination coefficient, $\sigma_0 = 4.5 \times 10^{-18} \text{ cm}^2$ as the effective cross section for resonant Ly α scattering and used the high redshift approximation for the Hubble constant, $H(z) = H_0 \Omega_{\text{mat}}^{1/2} (1+z)^{3/2}$.

3 THE INVERSION ALGORITHM

3.1 The basic iterative scheme

The proposed scheme for recovering the l.o.s. density from the flux is motivated by Lucy's method (Lucy 1974). In order to demonstrate the method let us, for the time being, consider the case where $\tau \ll 1$ and $v_{\text{p}} = 0$. In this case, we have

$$1 - F(w) = \int n_{\text{HI}}(x) G(w, x) dx. \quad (7)$$

This is a linear integral equation with a positive Kernel $G(w, x) = \mathcal{H}[w - x, b(x)] \sigma_0 c / H(z)$ and can be solved for n_{HI} using Lucy's iterative method. This is done in the following way. Divide w into equal bins of size Δw (the data are actually given in bins of w anyways) and set $f_i = 1 - F_i$. Provide an initial guess for $(n_{\text{HI}})_j$, say $(n_{\text{HI}})_j^0 = 1 - F_j H(z) / (\sigma_0 c)$. Denote the values of $(n_{\text{HI}})_j$ at the r th iteration by $(n_{\text{HI}})_j^r$ and evaluate the sum

$$f_i^r = \sum_j (n_{\text{HI}})_j^r G_{ij}^r \Delta w, \quad (8)$$

where

$$G_{ij}^r = \mathcal{H}[w_i - x_j, b_j^r] \frac{\sigma_0 c}{H(z)}. \quad (9)$$

The $(r+1)$ -th estimate of $(n_{\text{HI}})_j$ is then

$$(n_{\text{HI}})_i^{r+1} = \left[\frac{1}{2m+1} \sum_{k=i-m}^{i+m} (n_{\text{HI}})_k^r \right] \frac{\sum_j (f_j/f_j^r) \tilde{G}_{ij}}{\sum_j \tilde{G}_{ij}}, \quad (10)$$

where \tilde{G} is some Kernel which in principle may be chosen to be different from G . Lucy's method, however, uses $\tilde{G} = G$. The averaging over $2m+1$ adjacent bins mitigates the effect of noise in the data. We work with $m=3$.

Now we generalise the iteration scheme to the case where τ is not necessarily small. In this case, the relation between F and τ is nonlinear. However, since the relation is monotonic, we can still use a modified version of equation (10),

$$f_i^r = 1 - \exp\left[-\sum_j (n_{\text{HI}})_j^r G_{ij}^r \Delta w\right]. \quad (11)$$

How do we decide when to stop the iterations? Suppose that in the j -th bin, the $1\text{-}\sigma$ error in the measurement of F_j is σ_j . Let us define the quantity

$$\chi^2 = \sum_j \frac{1}{\sigma_j^2} (f_j - f_j^r)^2. \quad (12)$$

We choose to stop at the r -th iteration when the value of χ^2 drops below the number of data bins. It implies that the observed flux is consistent with being a noisy realisation of the reconstructed flux.

3.2 Recovery of the matter density in redshift space

We write (2) in terms of the redshift coordinate $s \equiv x + v_p(x)$, instead of x . If the coordinates x and s are related by a one-to-one mapping, then the velocity and the real space coordinate, can be expressed uniquely as functions of the redshift coordinate s . Working with s , equation (2) takes the following form

$$\begin{aligned} \tau(w) &= \sigma_0 \frac{c}{H(z)} \int_{-\infty}^{\infty} n_{\text{HI}}[s - v_p(s)] \left[1 - \frac{dv_p(s)}{ds} \right] \\ &\quad \mathcal{H}[w - s, b(s - v_p(s))] ds \end{aligned} \quad (13)$$

For brevity, we have maintained the same notation for the peculiar velocity as a function of s . According to the continuity equation, the density in redshift space, n_{HI}^s , is related to the density in real space by

$$n_{\text{HI}}^s(s) = n_{\text{HI}}[s - v_p(s)] \left[1 - \frac{dv_p(s)}{ds} \right]. \quad (14)$$

Therefore (13) becomes

$$\tau(w) = \int_{-\infty}^{\infty} K(w, s) n_{\text{HI}}^s(s) ds \quad (15)$$

where $K(w, s) = \mathcal{H}[w - s, b(s - v_p(s))] \sigma_0 c / H(z)$ and the iterative scheme described in the last section can be applied to obtain the redshift space density along the l.o.s. The parameter b depends on $(s - v_p)$ implicitly via n_{HI} . Because b

is a weak function of n_{HI} , we assume that b is constant in the reconstruction algorithm. This will greatly simplify the application of the algorithm. Tests of the algorithm, however, are done using mock spectra generated with varying b according to equation (4).

To relate the H I density to the matter density we use equation (3 and (6). We still need to know the value of \mathcal{A} to obtain $\rho_{DM}/\bar{\rho}_{DM}$. \mathcal{A} has been estimated by adjusting the mean flux of mock spectra generated from hydrodynamical simulations to match the mean flux of observed QSO absorption spectra (Rauch et al. 1997). The accuracy and possible biases of this determination have not yet been investigated in detail (see also Weinberg et al. 1997), but we consider the value of \mathcal{A} ($\propto (\Omega_{\text{bar}} h^2)^2 J^{-1} H(z)^{-1}$) to be presently known with about 30 percent accuracy. For most of the paper we therefore assume that we know the value of \mathcal{A} . In section 4.3 we show how the value of \mathcal{A} ($\propto (\Omega_{\text{bar}} h^2)^2 J^{-1} H(z)^{-1}$) can be estimated directly from the distribution of the recovered quantity $\mathcal{A}^{1/\alpha}(\rho_{DM}/\bar{\rho}_{DM})$ by assuming a parametric form for the probability distribution of the matter density.

3.3 From redshift space to real space

The correction for redshift distortions requires knowledge of the velocity field. The 3-dimensional velocity and mass density fluctuations are tightly related. However, non-linear velocity-density relations which are easy to implement generally relate real space quantities, as does the relation (3) between the H I and matter density. We have therefore to resort to an iterative procedure to derive the real space matter and H I densities from the estimated redshift space H I density. Two issues need to be stressed here: (i) the velocity field is not uniquely specified by the l.o.s. density field but influenced by the unknown 3D matter distribution, and (ii) redshift distortions can and do result in multi-valued zones where regions which do not overlap in real space are mapped onto the same redshift coordinate. In appendix A we describe a method which resembles Wiener filtering and addresses the first point. It allows us to obtain the most probable velocity field which is consistent with the estimated l.o.s. DM density field and has the statistical properties of a gravitationally clustering Gaussian random field of a given power spectrum. In principle the power spectrum can also be determined from the recovered density field but for simplicity we have chosen to adopt a power spectrum a priori. The results do not change much for reasonable choices of the assumed power spectrum. Multi-valued zones mainly occur in regions of high density where the inversion is difficult due to saturation effects in the spectrum. We did not try to correct for this effect, but discuss some of the biases introduced by peculiar velocities in section 4.

The iterative scheme to correct for redshift distortions which we have adopted can be summarized as follows:

- (i) Assume that the redshift-space and real-space H I density are equal and use (3) to compute the matter density field along the l.o.s.
- (ii) Estimate the peculiar velocity along the l.o.s. using the method described in the appendix.
- (iii) Use the estimated peculiar velocity field to correct for redshift distortions in the density field.

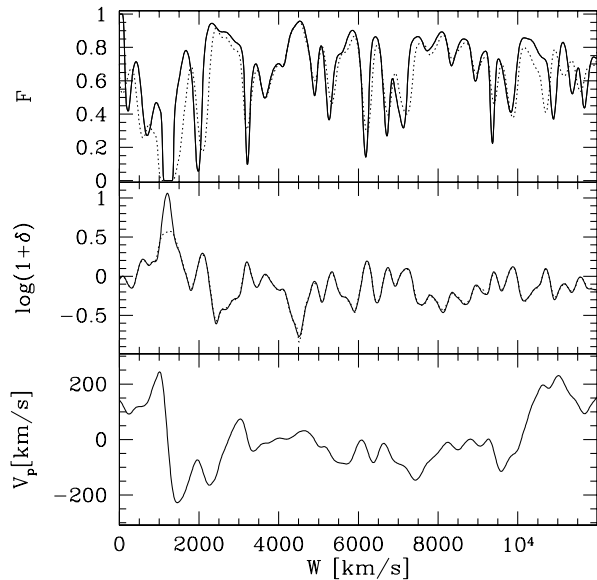


Figure 1. Normalized flux (top), density (middle) and velocity (bottom) along one line-of-sight through the simulation box at $z = 3$. The dotted curve in the top panel shows the flux with peculiar velocities set to zero and the dotted curve in the middle panel shows the corresponding recovered density field.

(iv) Use the corrected density field to obtain a better estimate for the peculiar velocity field.

(v) Repeat steps (ii)-(iv) until convergence is achieved.

The scheme proved to be efficient; it typically converges after a few iterations. Iterative schemes of this kind have been used for correcting redshift distortions in galaxy redshift survey (e.g. Yahil et. al. 1991).

4 TESTS WITH NUMERICAL SIMULATIONS

Ideally one would like to test the method with a large high-resolution hydrodynamical simulation of gas and dark matter. However, simulations of collisionless particles are still vastly superior in dynamical range and especially speed. We have therefore chosen to test our inversion algorithm with a high resolution N-body simulation of pure collisionless dark matter particles where we used the relations in section 2.1 to obtain the H I distribution from the smoothed dark matter density field. As demonstrated e.g. by Gnedin (1998) such a procedure results in a realistic H I distribution (apart from the high-density regions which are not of interest here).

The simulation used was run on the Cray T3E parallel supercomputer in Garching with a modified version (MacFarland et. al. 1997) of Couchman’s P^3M code (Couchman et. al. 1995). The initial conditions were generated from the power spectrum for a standard cold dark matter (CDM) universe with $\Omega = 1$ and $H_0 = 50\text{km/s}$ cubic box of comoving length of $60h^{-1}\text{Mpc}$. The simulation was normalised such that the linear *rms* density fluctuations in a sphere of 800km s^{-1} was 0.5 at redshift $z = 0$. The softening parameter was 13.2% of the mean particle separation and the mesh size was $N = 512$ in one dimension.

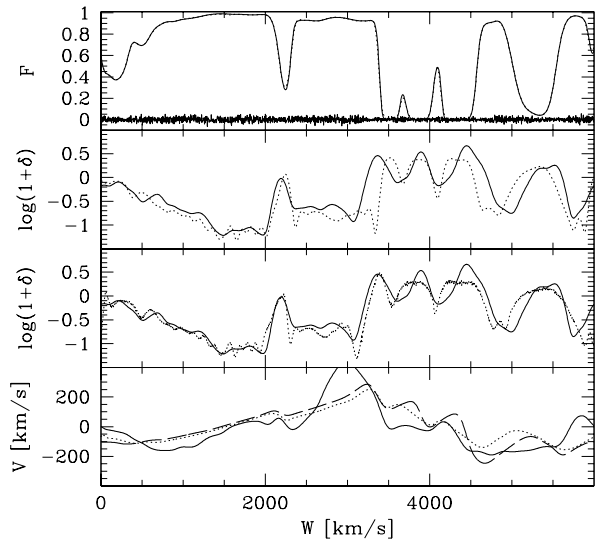


Figure 2. *Top panel:* Normalized flux (solid curve) in a line-of-sight through the simulation at $z = 0$ and the flux corresponding to the density and peculiar velocity field recovered with a Lucy-type inversion algorithm (dotted curve). The noise added to the input spectrum is shown separately at the bottom of the panel. *Second panel:* True real space density in the line-of-sight (solid curve) and recovered redshift-space matter density (dotted curve). *Third panel:* True real-space density (solid curve, same as in second panel) and real-space matter density recovered with applying redshift corrections (dotted curve). *Bottom:panel* The true l.o.s. peculiar velocity field (solid curve). The peculiar velocity estimated from the recovered density in redshift space (dotted curve). For comparison, also shown is the velocity recovered from the true real space density (dashed line).

4.1 Inverting mock spectra

We have generated mock spectra from velocity and density fields along lines of sight randomly drawn from the simulation box. We used the output of the simulation at two redshifts, $z = 3$ and $z = 0$, to investigate the effect of varying the fluctuation amplitude of the density field. We emphasize here that the mock spectra generated from the simulation at $z = 0$ are not meant to resemble absorption spectra at $z = 0$. The density and velocity fields in the simulations show significant variations in structure and amplitude at the two redshifts and the $z = 0$ spectra are investigated with the same mean flux as the $z = 3$ spectra in order to test the inversion algorithm under varying conditions.

Reliable velocity and density fields cannot be derived from the simulation on scales much smaller than the mean particle separation. We therefore applied Gaussian smoothing of widths $0.3h^{-1}\text{Mpc}$ and $0.6h^{-1}\text{Mpc}$, respectively, to the outputs of the simulation at $z = 3$ and $z = 0$. Both smoothing scales correspond to the same physical scale (60km s^{-1}). The *rms* values of the smoothed density fluctuations were 0.89 and 3.52, respectively. The density of neutral hydrogen was assumed to follow the relation (3) with $\alpha = 1.7$. The absorption optical depth was computed according to equation (2), (3), and (4) with $b_0 = 30\text{km s}^{-1}$. For both redshifts the value of \mathcal{A} was adjusted so that the mean normalized flux of a large ensemble of mock spectra

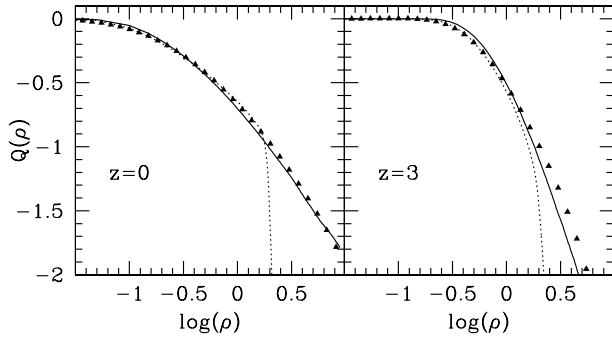


Figure 3. The cumulative probability distribution of the true density field (solid curve) and that of the density field recovered (dotted curve) from mock spectra generated from the simulation at $z = 0$ (left) and $z = 3$ (right). The triangles are the corresponding parametric form derived from an Edgeworth expansion of the PDF (17) as explained in the text.

was 0.69 (about the observed mean flux at $z = 3$ as determined by Rauch et al. 1997). The spectra were convolved with a Gaussian of 8km/s FWHM to mimic instrumental broadening and photon/read-out noise was added with a total S/N=50 per 3km/s pixel.

The solid curve in the top panel of Fig.1 is a mock spectrum generated from the simulation output at $z = 3$. The dotted curve is the same spectrum with the peculiar velocities set to zero. The peculiar motions do not only introduce a systematic shift but also a narrowing of the absorption features (see also Weinberg et al. 1998 for a discussion of this point). Furthermore, unsaturated lines get deeper due to the enhanced clustering in redshift space. The mean flux is also affected. For constant \mathcal{A} it increased from 0.66 to 0.69 including peculiar motions while the rms flux fluctuations increased from 0.31 to 0.35.

Figure 2 shows some typical results of our inversion procedure. In the top panel a mock spectrum is plotted (solid line) together with the spectrum corresponding to a recovered density and peculiar velocity field (dotted line). The smoothness of the dotted curve demonstrates that our inversion procedure succeeds in mitigating the noise in the data (which for clarity is shown separately at the bottom of the panel).

Let us now have a look at the DM density field recovered from a mock spectrum generated with no peculiar velocities as shown in the middle panel of Figure 1. In this case the correspondence is excellent up to densities where the absorption features become heavily saturated (for Ly α absorption at a overdensity of about 3 at $z = 3$). Without peculiar velocities our inversion procedure works as well as we could reasonably expect. The obvious way to extend the inversion procedure to regions of higher density would be to use the higher order Lyman series lines which have smaller effective absorption cross sections and therefore saturate at increasingly higher densities (Cowie, private communication). However, as we discuss below peculiar velocities significantly affect the quality of the recovered density field, especially in high density regions. The incorporation of higher order Lyman series lines in the inversion procedure will therefore be difficult and we leave this to future work.

The second panel of Fig. 2 shows the DM density field recovered from a mock spectrum generated with peculiar velocities but before correcting for redshift distortions. As expected the correspondence between true and recovered density is degraded compared to the case where the spectrum was generated with the peculiar velocities set to zero. The main features of the density field are still recovered but there is a significant shift between true and recovered density in real space and there of course remains the systematic underestimate of the density in saturated regions.

The third panel shows the reconstructed density for our full iterative procedure including the correction of redshift distortions as described in section 2.4. The shift between true and recovered density in real space is reduced and the overall correspondence has significantly improved. This indicates that we succeed in removing a major fraction of the redshift space distortions. The recovered and true l.o.s. velocity fields are shown in the bottom panel. In all cases shown we have used the correct value for \mathcal{A} , i.e. the value used to generate the mock spectrum. It should have become clear in this section that peculiar velocities significantly influence the quality of the recovery.

4.2 The density probability distribution

For a statistical analysis of the recovered density field we will use the probability distribution function in differential (PDF) and cumulative form (CPDF). Let us for the time being still assume that the true value of \mathcal{A} is known. We will discuss how \mathcal{A} can be estimated from the PDF of the recovered density field in the next section.

Fig. 3 shows the CPDF for the true and recovered DM density field for the simulations at $z = 3$ and $z = 0$. At low densities both curves correspond very well but the deviations become large at high densities due to saturation effects which confirms the visual impression from figure (1) and (2). We further quantify the differences between the CPDFs of true and recovered density in terms of a number of moments of the density distribution in table 1. The bias in the recovered density introduces large discrepancies between the estimated and true values of the moments. For example, the mean and rms values estimated at $z = 0$ are: 0.614 and 0.608; instead of the true values: 1 and 3.52.

What we would like to have is a simple parametric form for the PDF of the DM density. This could then be used to correct for the biases in the recovered density field. It has been suggested (e.g. Kofman et. al. 1994, Coles & Jone 1991.) that the PDF of the density field of a gravitationally clustering Gaussian random field in the mildly non-linear regime is well described by a *log-normal* PDF. In that case the quantity

$$\nu \equiv [\ln(1 + \delta) - \mu_1]/\mu_2 \quad (16)$$

has a normal (Gaussian) PDF, where μ_1 and μ_2 are the average and *rms* values of $\ln(1 + \delta)$. In figure (4) we compare the PDF of the DM density in the simulations (filtered with Gaussian windows of widths $R_s = 1.2\text{Mpc}$ and $R_s = 5\text{Mpc}$ in comoving units for $z = 0$ and $z = 3$) with a log-normal distribution. For large smoothing scale the density field is indeed adequately described by a log-normal distribution. However, for decreasing smoothing scale, the true PDF becomes more and more skewed. The skewness of ν which we

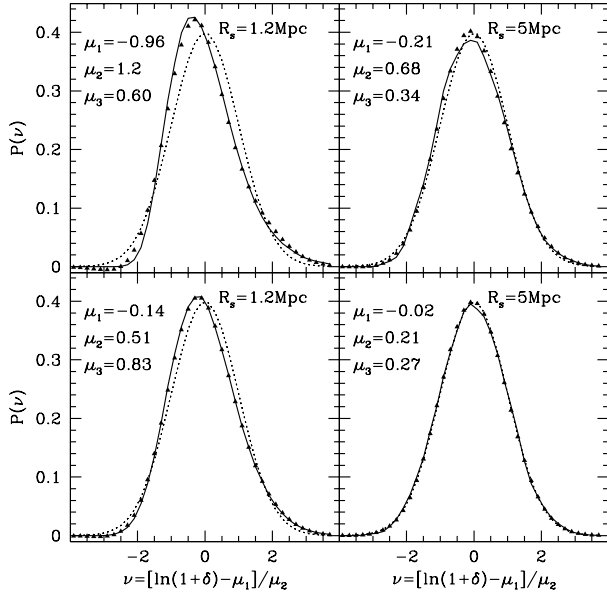


Figure 4. The probability distribution of DM density in the simulation at $z = 0$ (top panels) and $z = 3$ (bottom panels) in terms of $\nu = [\ln(1 + \delta) - \mu_1] / \mu_2$ (the density field was smoothed with a Gaussian windows of width 1.2Mpc and 5Mpc in comoving units, respectively). The moments $\mu_1 = \langle x \rangle$, $\mu_2 = \langle (x - \mu_1)^2 \rangle^{1/2}$ and $\mu_3 = \langle (x - \mu_1)^3 \rangle / \mu_2^3$, where $x = \ln(1 + \delta)$, are indicated on the plot. The dotted curves are the best-fitting log-normal distribution, while the triangles show the best-fitting Edgeworth expansion of the PDF as in equation (17).

Table 1. Moments of the density field. The symbols $\langle \cdot \rangle$ and $|\cdot|$ denote average and absolute values respectively. Also $x = \delta / \sigma$, where $\delta = \rho / \langle \rho \rangle - 1$. The *top* figures are for the true density field, the *middle* figures are for the recovered density field and the *bottom* figures are for the best-fitting Edgeworth expansion as described in the text. The moments are computed assuming the true value of \mathcal{A} .

	$\rho / \langle \rho \rangle$	σ	$S_3 = \langle x^3 \rangle / \sigma^3$	$S_{3r} = \langle x ^3 \rangle$	$S_{4r} = \langle x ^4 \rangle$
True					
z=3:	1	0.89	4.85	0.66	0.61
z=0:	1	3.52	5.08	0.93	0.33
Rec					
z=3:	0.80	0.51	2.25	0.36	0.79
z=0:	0.61	0.61	1.97	0.40	0.83
Fit					
z=3:	1	1.12	4.27	0.69	0.59
z=0:	1	2.97	8.75	0.85	0.37

define as $\mu_3 = \langle \nu^3 / \mu_2 \rangle$ is one way of quantifying the deviation from a log-normal distribution and is also indicated on the plot.

To obtain an improved fit to the PDFs of our simulation we use the first term of an Edgeworth expansion (Colombi 1994, Juszkiewicz et. al. 1995),

$$P(\nu) = G(\nu) \left[1 + \frac{1}{3!} \mu_3 \mu_2 (\nu^3 - 3\nu) \right], \quad (17)$$

where $G(\nu)$ is a Gaussian with zero mean and unit variance. By imposing the condition $\langle \delta \rangle = 0$ we find the following relation between the three parameters,

$$\mu_1 + \frac{\mu_2^2}{2} + \ln \left(1 + \frac{\mu_2^4 \mu_3}{3!} \right) = 0. \quad (18)$$

The functional form (17) has therefore two free parameter (one more than a log-normal PDF). In the remainder of this section we arbitrarily choose to work with μ_2 and μ_3 . We also tried to reduce (17) to a one-parameter family. We failed, however, at establishing a tight relation between the two parameters for the PDFs of our simulations, which holds at all redshifts (see also Colombi 1994).

In practice we find it again more convenient to work with the CPDF rather than the PDF itself,

$$\begin{aligned} Q(\rho) &\equiv \int_{\rho}^{\infty} P(\nu) d\nu \\ &= \frac{1}{2} \operatorname{erfc} \left(\frac{\nu}{\sqrt{2}} \right) + \frac{\mu_2 \mu_3}{3! \sqrt{2\pi}} (\nu^2 - 1) \exp \left(-\frac{\nu^2}{2} \right). \end{aligned} \quad (19)$$

We fit the functional form (19) for the CPDF with μ_1 expressed in terms of μ_2 and μ_3 (18) to $Q_0(\rho)$ (the CPDF computed directly from the recovered density) by minimizing the quantity

$$R = \int_0^{\rho_{\max}} d\rho [Q(\mu_2, \mu_3; \rho) - Q_0(\rho)]^2. \quad (20)$$

with respect to μ_2 and μ_3 . The cutoff ρ_{\max} is introduced in order to give no weight to high-density regions where the discrepancy between the recovered and true densities is severe. Fig. 3 and Fig. 4 show these fits as triangles. The quality of the fit is generally satisfying. At the bottom of table 1 we list the corresponding moments. The mean is correctly recovered by construction but the other moments are also in significantly better agreement with the moments of the true density field than those calculated directly from the recovered density field. The rms value at $z = 0$ is now e.g. 2.97 as compared to 0.62 from direct calculation and 3.52 for the true density field. When we fitted a log-normal distribution to the CPDF we found similar values for the moments as for the Edgeworth expansion.

4.3 Determining \mathcal{A} ($\propto \Omega_{\text{bar}}^2 / J$)

So far we have assumed that we know the value of \mathcal{A} . As is clear from equation (3) and (6) assuming a wrong value of \mathcal{A} leads to an estimate of $\rho_{DM} / \bar{\rho}_{DM}$ which is wrong by a constant factor $(\mathcal{A} / \mathcal{A}_{\text{true}})^{1/\alpha}$ independent of the density. It is therefore possible to directly estimate \mathcal{A} by fitting one of the parametric forms discussed in the last section to the CPDF of the recovered density with \mathcal{A} being left as an additional free parameter. It turned out that the Edgeworth expansion is less suitable for this procedure as it already has two free parameters (it becomes then sometimes difficult to get a unique fit). Fig. 5 shows the residuals of such a fit for the log-normal distribution as a function of \mathcal{A} at the two redshifts. The residuals change significantly with varying \mathcal{A} and show pronounced minima but the values of \mathcal{A} at the minima are biased low by about 25 percent and 15 percent,

Table 2. Sensitivity of the estimated \mathcal{A} and the moments to uncertainties in α . The bottom line shows the effect of varying the mean flux from 0.69 (as in table 1) to 0.75 ($\alpha = 1.7$ was assumed). Results are for $z = 0$.

	\mathcal{A}_{\min}	μ	σ	S_3	S_{3r}	S_{4r}
$\alpha = 2.0$	0.72	1	2.00	6.35	0.82	0.46
$\alpha = 1.7$	0.84	1	2.97	8.75	0.85	0.37
$\alpha = 1.5$	1.08	1	3.70	15.64	0.82	0.31
$\langle F \rangle = 0.745$	1	0.92	2.89	8.89	0.85	0.37

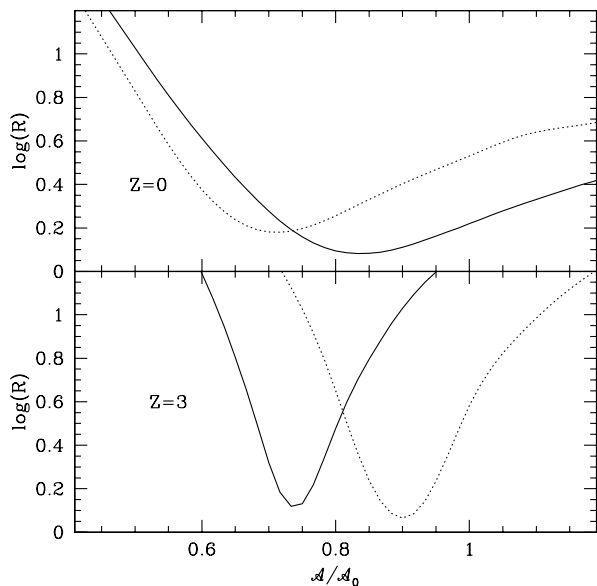


Figure 5. Residuals of the fit of a log-normal distribution to the distribution function of the recovered density as a function of the ratio of assumed to true value of \mathcal{A} . Solid and dotted lines refer to mock spectra generated with and without peculiar velocities, respectively.

respectively. The error of \mathcal{A} determined in this way is probably of the same order as when \mathcal{A} is estimated by adjusting the mean flux level in mock spectra generated from numerical simulations. We also show the case for a recovery from mock spectra with the peculiar velocities set to zero (dotted curves). The minima shift significantly. This demonstrates that the bias in \mathcal{A} is not only due to the systematic underestimate of the density in high-density regions and the inaccuracy of the log-normal distribution but also due to the effect of peculiar velocities. Peculiar velocities introduce a dependence of the bias on the amount of small-scale power in the density fluctuation spectrum as apparent from the comparison between the cases at $z = 3$ and $z = 0$ which differ by a factor four in the rms density fluctuations. More numerical work is needed to quantify the effect of changing the cosmological model/power spectrum and the resolution, but it seems nevertheless feasible to correct for the bias in \mathcal{A} to about 10 percent accuracy.

The assumed value of \mathcal{A} will obviously also affect the determination of the moments described in the last section.

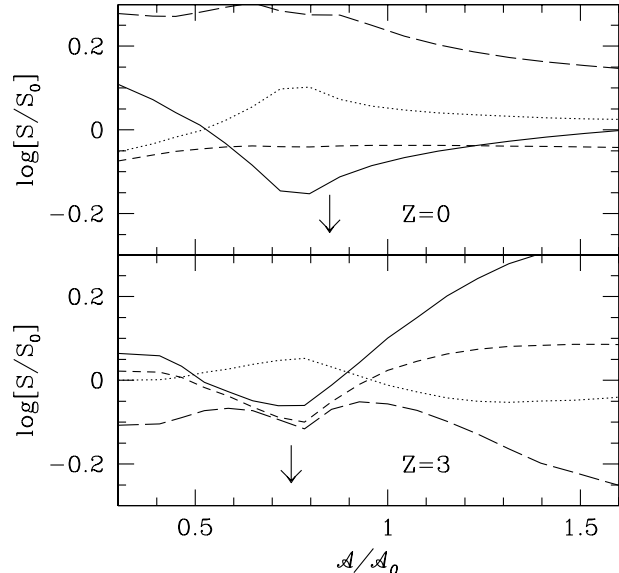


Figure 6. Moments of the density probability distribution determined by fitting an Edgeworth expansion as a function of the assumed value of \mathcal{A} . All values are divided by their true values. Solid, long-dashed, short-dashed and dotted lines correspond to σ , S_3 , S_{3r} and S_{4r} as defined in table 1. The arrows indicate the position of the minima in Fig. 5 for the case with peculiar velocities.

Figure 6 shows the dependence of the estimated moments on the assumed value of \mathcal{A} . For a reasonable range of \mathcal{A} the biases range from 20 to 50 percent. If \mathcal{A} is determined by fitting a log-normal CPDF and the moments are then estimated by fitting an Edgeworth expansion to the CPDF with this value of \mathcal{A} the biases in the moments are generally smaller than 25 percent.

We have also run our inversion procedure with equation of states different from the one used to generate the mock spectra and changed the mean flux in order to test how sensitive the biases are to these parameters. The corresponding estimates of \mathcal{A} and the moments are listed in table 2. At least for the parameter space explored the biases seem to be robust.

5 DISCUSSION AND CONCLUSIONS

We have used numerical simulations to demonstrate that the l.o.s. matter density field can be recovered from QSO absorption spectra using an analytical model for the IGM and a Lucy-type iterative inversion algorithm. We have thereby estimated the l.o.s. peculiar velocity field from the recovered density field and have corrected for redshift distortions in an iterative procedure. The inversion works well for the most underdense regions up to the density where the absorption features saturate. For Ly α this occurs at an overdensity of a few but this limit can be pushed to higher densities by incorporating higher order lines of the Lyman series. However, an inversion will become increasingly more difficult at higher densities due to shell crossing and shock heating of the gas.

We have then used the fact that the density probability distribution seems to have a universal shape to get reliable estimates of higher order moments of the PDF despite the missing high-density tail. We found that the Edgeworth expansion is an excellent approximation to the PDF of the logarithm of the density, consistent with the results of Colombi (1994). By fitting the first two terms of such an Edgeworth expansion we estimated a number of moments of the PDF with an accuracy of about 25 percent. Estimates of similar accuracy were obtained for the parameter combination $(\Omega_{\text{bar}} h^2)^2 J^{-1} H(z)^{-1}$ by fitting to a log-normal distribution. We expect that, eventually, these biases can be corrected to 10 percent accuracy.

In principle it should also be possible to estimate the correlation function and the power spectrum directly from the recovered density field. These will, however, be affected by peculiar motions, the inability to recover high density regions and the bias in the determination of \mathcal{A} . We have not yet investigated in detail how big the resulting errors are. It might well be that a comparison of observed flux power spectra with those of mock spectra as suggested by Croft et al. is the most favourable way to deal with these problems.

Observational information on the PDF of the matter density comes so far mainly from the analysis of galaxy surveys and is restricted to small redshifts. These constraints could be checked and extended to a much wider redshift range by applying our inversion technique to a moderate number of QSO absorption spectra of the kind which are now routinely taken with 10m class telescopes. This should also check and tighten existing constraints on the evolution of the UV background. By combining our inversion technique with a redshift survey along QSO sightlines the clustering of galaxies and matter can be related without referring to a particular cosmological model. Such a determination of the bias between galaxy and matter clustering is especially worthwhile. Most currently favoured models agree with the recently determined clustering strength of high-redshift galaxies but differ strongly in their predictions for the yet unknown bias relation (Adelberger et al. 1998). Three-dimensional information on the density and peculiar velocity field can be gained by applying the method to two or more spatially close line-of-sights. An intermediate-resolution spectral survey of quasars down to about 22nd magnitude in a field of a couple of square degree size has e.g. been suggested as a possible project for the VLT (Petitjean 1996). Such a survey will result in about 100 l.o.s. in a region about 30Mpc across. With the method proposed in the appendix such a region could become a unique laboratory for the study of how galaxy formation is related to the distribution and dynamics of the underlying matter field.

6 ACKNOWLEDGMENTS

We thank Rupert Croft, Michael Rauch, Ravi Sheth, David Weinberg and Simon White for helpful comments. AN thanks Yehuda Hoffman for many discussions on constrained realisations. This work was supported in part the EC TMR network for "galaxy formation and evolution" and the "Sonderforschungsbereich 375-95 für Astro-Teilchenphysik der Deutschen Forschungsgemeinschaft".

REFERENCES

- Adelberger K.L., Steidel C.S., Giavalisco M., Dickinson M.E., Pettini M., Kellog M., 1998, ApJ, in press, astro-ph/9804236
 Bahcall J.N., Salpeter E.E 1965, ApJ , 142, 1677
 Bechtold J., Crofts A.P.S., Duncan R.S., Fang Y., 1994, ApJ, 437, L83
 Bi H.G., Börner G., Chu Y. 1992, A&A, 266, 1
 Bi H.G., 1993, ApJ, 405, 479
 Bi H.G., Davidsen A.F., 1997, ApJ, 479, 523
 Bond J.R., Szalay A.S., Silk J., 1988, ApJ, 324, 627
 Cen R., Miralda-Escudé J., Ostriker J.P., Rauch M., 1994, ApJ, 437, L9
 Coles, P., Jones, B.J.T, 1991, MNRAS, 248, 1
 Colombi, S., 1994, ApJ, 435, 536
 Cooke A.J., Espey B., Carswell R.F., 1997, MNRAS, 284, 552
 Couchman H.M.P., Thomas P.A., Pearce F.R., 1995, ApJ, 452, 797
 Dinshaw N., Impey, C.D., Foltz C.B., Weymann R.J., Chaffee F.H., 1994, ApJ, 437, L87
 Fisher K.B., Lahav O., Hoffman Y., Lynden-Bell D., Zaroubi S., 1995, MNRAS, 272, 885
 Gnedin N., Hui L., 1998, MNRAS, in press, astro-ph/9706219
 Gunn J.E., Peterson B.A., 1965, ApJ, 142, 1633
 Haehnelt M., Steinmetz M., 1998, MNRAS, in press, astro-ph/9706296
 Hernquist L., Katz N., Weinberg D.H., Miralda-Escudé J., 1996, ApJ, 457, L51
 Hui L., Gnedin N.Y., 1997, MNRAS, 292, 27
 Hoffman, Y., Ribak, E., 1991, ApJ, 380L, 5
 Jenkins A., Frenk, C.S., Pearce, F.R., Thomas, P.A., Colberg, J.M., S.D.M., Couchman, H.M.P., Peacock, J.A., Efstathiou, G., Nelson, A.H., 1998, ApJ, in press, astro-ph/9709010.
 Lucy L. B., 1974, *Astronomical J.* 79, 745
 MacFarland T.J., Couchman H.M.P., Pearce F.R., Pichlmeier J., 1998, astro-ph/9805096
 McGill C., 1990, MNRAS, 242, 544
 Miralda-Escudé J., Cen R., Ostriker J.P., Rauch M., 1996, ApJ, 471, 582
 Nusser A., Dekel A., Bertschinger E., Blumenthal G., 1991, *Astrophys. J.* 379 6
 Petitjean P., Mucket J.P., Kates R.E., 1995, A&A, 295, L9
 Petitjean P., 1997, in: The Early Universe with the VLT, ed. Bergeron J., ESO Workshop, Springer, p.266
 Rauch M., Miralda-Escudé J., Sargent W.L.W., Barlow T.A., Weinberg D.H., Hernquist H., Katz N., Cen R., Ostriker J.P. 1997, ApJ, 489, 7
 Rauch M., 1998, ARAA, in press
 Sigad, Y., Eldar, A., Dekel, A., Strauss, M.A., Yahil, A., 1998, ApJ, 495, 516
 Wechsler, R.H., Gross, M.A.K., Primack, J.R., Blumenthal, G.R., Dekel, A., 1998, ApJ, in press, astro-ph/9712141
 Weinberg D.H, 1992, MNRAS, 254, 315
 Weinberg D.H, Miralda-Escudé J., Hernquist L., Katz, N., 1997, ApJ, 490, 564
 Weinberg D.H, Miralda-Escudé J., Hernquist L., Katz N., Miralda-Escudé J., 1998, in: Structure and Evolution of the IGM from QSO absorption lines, eds. Petitjean P., Charlot S., Editions Frontieres, p. 133
 Wiener, N. 1994, in *Extrapolation and Smoothing of Stationary Time Series*, (New York, Wiley)
 Yahil, A., Strauss, M.A., Davis, M., Huchra, J.P., 1991, ApJ, 372, 380
 Zaroubi S., Hoffman Y., Fisher K.B., Lahav O., 1995, ApJ, 449, 446
 Zhang Y., Anninos P., Norman M.L., 1995, ApJ, 453, L57

APPENDIX A: PECULIAR VELOCITIES AND 3-D DENSITIES FROM LINE-OF-SIGHT DENSITY FIELDS

A1 From l.o.s. density to l.o.s. peculiar velocity

In this section we describe the method which we used to estimate the l.o.s. peculiar velocity component from the (estimated) *real* space density along the l.o.s. We first have to assume a non-linear relation between the 3-dimensional velocity and density fields. Various such relations have been suggested, here we work with the relation found empirically by Nusser et. al. (1991). Let $\theta = -\text{div}\mathbf{v}$, where \mathbf{v} is the physical peculiar velocity and the divergence is with respect to the physical coordinate r in units of km/s. The approximation suggested by Nusser et al. (1991) is given by

$$\theta = \frac{\delta}{1 + 0.18\delta} + \text{const.} \quad (\text{A1})$$

The relation is local and provides θ in terms of the density contrast along the l.o.s. The constant factor is introduced to ensure $\langle \theta \rangle = 0$. Since θ involves derivatives of velocity components perpendicular to the l.o.s., the l.o.s. peculiar velocity component can not uniquely be determined from θ . Therefore, the best we can do is provide an estimate for the l.o.s. peculiar velocity based on some statistical assumptions. Neither of the fields θ or δ is Gaussian. However, for an approximate treatment we assume here that θ is Gaussian. Note that by (A1) this assumption does not imply Gaussian density fluctuations. At the end of the next subsection we will briefly describe how estimates of the peculiar velocity can be obtained without assuming that the field θ is Gaussian. Let v be the component of \mathbf{v} along the l.o.s. Subsequently we work with the (1-dimensional) Fourier transforms, $\tilde{\theta}(q)$ and $\tilde{v}(q)$ of the l.o.s. fields v and θ . According to Bi (1993) $\tilde{\theta}$ and \tilde{v} are related by

$$\tilde{\theta}(q) = \tilde{u}(q) + \tilde{w}(q), \quad (\text{A2})$$

$$v(q) = iq\alpha(q)\tilde{w}(q), \quad (\text{A3})$$

where $\tilde{w}(q)$ and $\tilde{u}(q)$ are two uncorrelated Gaussian fields with power spectra P_w and P_u . These power spectra can be written, in terms of the 3D matter power spectrum P ,

$$P_w(q) = 2\pi\alpha^{-1} \int_q^\infty P(k)k^{-1} dk, \quad (\text{A4})$$

and

$$P_u(q) = 2\pi \int_q^\infty P(k)k dk - P_w(q), \quad (\text{A5})$$

with

$$\alpha(q) = \frac{\int_q^\infty P(k)k^{-3} dk}{\int_q^\infty P(k)k^{-1} dk}. \quad (\text{A6})$$

The relations (A2) and (A3) can be used to estimate $\tilde{v}(q)$ from $\tilde{\theta}(q)$. For simplicity, we work with \tilde{w} instead of \tilde{v} and switch back to \tilde{v} at the end of the calculation. According to Bayes' theorem the conditional probability $P_r[w|\tilde{\theta}]$ is given by

$$P_r(w|\tilde{\theta}) = \frac{P(w)}{P(\tilde{\theta})} P(\tilde{\theta}|w) \quad (\text{A7})$$

Using the relations (A2) and (A3) we find

$$P_r(\tilde{\theta}|w) \propto \exp\left[-\frac{(\tilde{\theta} - w)^2}{2P_u}\right], \quad (\text{A8})$$

and

$$P_r(\tilde{w}) \propto \exp\left[-\frac{w^2}{2P_w}\right]. \quad (\text{A9})$$

Therefore

$$P_r(\tilde{w}|\tilde{\theta}) \propto \exp\left[-\frac{(\tilde{\theta} - \tilde{w})^2}{2P_u} - \frac{\tilde{w}^2}{2P_w}\right] \quad (\text{A10})$$

This is a Gaussian with mean

$$\langle \tilde{w}|\tilde{\theta} \rangle = \left(1 + \frac{P_u}{P_w}\right)^{-1} \tilde{\theta}, \quad (\text{A11})$$

and variance (power spectrum)

$$P_{w|\tilde{\theta}} = \frac{P_w^2}{P_u + P_w}. \quad (\text{A12})$$

Thus, given $\tilde{\theta}(q)$, one may write

$$\tilde{w}(q) = \left(1 + \frac{P_u}{P_w}\right)^{-1} \tilde{\theta} + n(q), \quad (\text{A13})$$

where $n(q)$ is a random Gaussian variable with power spectrum $P_{w|\tilde{\theta}}$ which is uncorrelated with $\tilde{\theta}(q)$. The form of (A11) is reminiscent of Wiener filtering of noisy data (Wiener 1949, see also Zaroubi et. al. (1995) and Fisher et. al. (1995) for applications to cosmology). To see this simply identify P_u and P_w as, respectively, the signal and noise power spectra. According to (A2), the power spectrum of the unconditional $\tilde{\theta}$ is $P_\theta = P_w + P_u$. This clearly differs from the power spectrum of $\langle \tilde{w}|\tilde{\theta} \rangle$ given in (A12). Following Sigad et. al. (1998) here we replace the filter $(1 + P_u/P_w)^{-1}$ in (A11) by $(1 + P_u/P_w)^{-1/2}$ in order to preserve the power spectrum of the unconditional field. Alternatively we could have complemented $\langle \tilde{w}|\tilde{\theta} \rangle$ with the random field $n(q)$ in order to preserve the power.

A2 Reconstruction of 3D fields

For simplicity we discuss the case of a single l.o.s. The generalisation to multiple parallel lines of sight is obvious. We arbitrarily choose the l.o.s. to be along the x axis. Once the density δ^{los} in the l.o.s. is given, we can easily compute the corresponding Fourier transform $\tilde{\delta}^{\text{los}}(q)$ defined by

$$\tilde{\delta}^{\text{los}}(q) = \frac{1}{(2\pi)^{1/2}} \int \delta^{\text{los}}(x) \exp(iqx) dx \quad (\text{A14})$$

We write the 3D density field $\delta(\mathbf{r})$ in terms of its Fourier transform

$$\delta(\mathbf{r}) = \frac{1}{(2\pi)^{3/2}} \int \tilde{\delta}(\mathbf{k}) \exp(-i\mathbf{k} \cdot \mathbf{r}) d^3\mathbf{k}. \quad (\text{A15})$$

Define $l(x) = \delta(\mathbf{r} = x\hat{x})$ where \hat{x} is a unit vector along the x -axis. Hence, by combining (A14) and (A15) we obtain

$$\begin{aligned} \tilde{\delta}^{\text{los}}(q) &= \frac{1}{(2\pi)} \int \tilde{\delta}(k_{\parallel}, \mathbf{k}_{\perp}) \exp(iqx - ik_{\parallel}x) dk_{\parallel} d^2\mathbf{k}_{\perp} dx \\ &= \int \tilde{\delta}(q, \mathbf{k}_{\perp}) d^2\mathbf{k}_{\perp}, \end{aligned} \quad (\text{A16})$$

where k_{\parallel} and \mathbf{k}_{\perp} are the components parallel and perpendicular to the l.o.s. The problem of reconstructing the 3D

density field reduces to estimating $\tilde{\delta}(\mathbf{k})$ given the coefficients $\tilde{\delta}^{\text{los}}(q)$ and the relation (A16). Note that $\tilde{\delta}^{\text{los}}$ can be computed from δ^{los} . The method of Hoffman and Riback (1991) (hereafter HR) can be used to obtain such an estimate. First, we derive an expression for the mean value $\tilde{\delta}^{\text{MV}}(\mathbf{k}) = \langle \tilde{\delta}(\mathbf{k}) | \{\tilde{\delta}^{\text{los}}(q)\} \rangle$ of $\tilde{\delta}(\mathbf{k})$ corresponding to a particular \mathbf{k} given the set of coefficients $\{\tilde{\delta}^{\text{los}}(q)\}$. According to HR, we have

$$\tilde{\delta}^{\text{MV}}(\mathbf{k}) = \int M(\mathbf{k}, q') N^{-1}(q, q') \tilde{\delta}^{\text{los}}(q) dq dq', \quad (\text{A17})$$

where $M(\mathbf{k}, q') = \langle \tilde{\delta}(\mathbf{k}) \tilde{\delta}^{\text{los}}(q) \rangle$ is the covariance matrix of $\tilde{\delta}$ and $\tilde{\delta}^{\text{los}}$, and $N^{-1}(q, q')$ is the *inverse* of the covariance matrix $N(q, q') = \langle \tilde{\delta}^{\text{los}}(q) \tilde{\delta}^{\text{los}}(q') \rangle$; both matrices are of infinite dimension. Using the homogeneity condition, $\langle \tilde{\delta}^{\text{los}}(\mathbf{k}) \tilde{\delta}^{\text{los}}(v\mathbf{k}') \rangle = \delta^{\text{D}}(\mathbf{k} - \mathbf{k}') P(k)$ and the relation (A16) it can be seen that N and M are given by

$$N(q, q') = \delta^{\text{D}}(q - q') P^{\text{los}}(q), \quad (\text{A18})$$

and

$$M(\mathbf{k}, q) = \delta^{\text{D}}(q - k_{\parallel}) P\left(\sqrt{q^2 + \mathbf{k}_{\perp}^2}\right) \quad (\text{A19})$$

where δ^{D} is the Dirac δ -function and

$$P^{\text{los}} = 2\pi \int_q^{\infty} P(k) k dk \quad (\text{A20})$$

is the 1D power spectrum of the density field along the l.o.s. The mean is given by

$$\tilde{\delta}^{\text{MV}}(\mathbf{k}) = \frac{P(k)}{P^{\text{los}}(k_{\parallel})} \tilde{\delta}^{\text{los}}(k_{\parallel}). \quad (\text{A21})$$

Once the mean values are given, a constrained random realisation, $\tilde{\Delta}^{\text{C}}$ can be generated from an unconstrained random realisation $\tilde{\Delta}$ using (HR),

$$\tilde{\Delta}^{\text{C}}(\mathbf{k}) = \tilde{\Delta}(\mathbf{k}) + \frac{P(k)}{P^{\text{los}}(k_{\parallel})} [\tilde{\delta}^{\text{los}}(k_{\parallel}) - \tilde{\Delta}^{\text{los}}(k_{\parallel})], \quad (\text{A22})$$

where $\tilde{\Delta}^{\text{los}}(k_{\parallel})$ are the 1D Fourier coefficients of the unconstrained density field in the l.o.s.

The treatment so far relied on the HR method which assumes Gaussian fields. This treatment will not be satisfactory for a 3D reconstruction in the non-linear regime. The unconstrained density field as given by (A22) is e.g. not guaranteed to have positive values everywhere. The scheme can be extended to the non-linear regime by two modifications: (i) use $\ln(1 + \delta)$ instead of δ , (ii) extract an unconstrained random field $\Delta(\mathbf{r})$ or its Fourier transform $\tilde{\Delta}(\mathbf{k})$ from a fully non-linear N-body simulation. The simulations can be used to compute the 1D and 3D power spectra of $\ln(1 + \delta)$ which are required to generate the constrained realisation. But note that these power spectra can in principle be estimated from the density field along the l.o.s.

A 3D constrained realisation obtained with this scheme adapted to the non-linear regime can then be used to estimate the peculiar velocity without assuming θ to be Gaussian. θ can be computed at any point in space from the 3D constrained realization of the density field using the velocity-density relation (A1) and assuming a potential flow. The peculiar velocity is then obtained by solving a Poisson-like equation to recover θ . The implementation of this alternative scheme for recovering the peculiar velocity field and a

comparisons to the scheme described in the last section is left to future work.